Physics-Constrained Deep Learning of Geomechanical Logs

Yuntian Chen and Dongxiao Zhang

***Abstract*— Geomechanical logs are of ultimate importance for subsurface description and evaluation, as well as for the exploration of underground resources, such as oil and gas, groundwater, minerals, and geothermal energy. Together with geological and hydrological properties, low-cost and high-accuracy models can be generated based on geomechanical parameters. However, it is challenging to directly measure geomechanical parameters, and they are usually estimated based on other measured quantities. For example, geomechanical logs may be obtained with certain empirical models from sonic logs together with prior information such as rock types, which are not readily available. Finding a way to directly estimate geomechanical logs based on easily available conventional well logs can result in significant cost savings and increased efficiency. In this article, we showed that deep learning via the long short-term memory network (LSTM) is effective in constructing an end-to-end model that takes the spatial dependence in well logs into consideration. We further proposed a physics-constrained LSTM, in which the physical mechanism behind the geomechanical parameters is utilized as *a priori* information. This state-of-the-art model is capable to directly estimate geomechanical logs based on easily available data, and it achieves higher prediction accuracy since the domain knowledge of the problem is considered.**

***Index Terms*— Geomechanical parameters, long short-term memory network (LSTM), physics-constrained, physics-informed, well logs.**

I. Introduction

WELL logging is an essential tool for formation description and resource evaluation for exploration of oil and gas, groundwater, mineral and geothermal energy, and environmental and geotechnical studies [1]–[3]. Obtaining geomechanical logs is extremely important for building an accurate model, improving formation evaluation accuracy, and optimizing well drilling and completion strategies. Since accurate measurement of geomechanical logs relies on expensive and time-consuming operations, such measurements are often lacking in actual resource recovery processes.

Manuscript received April 19, 2019; revised August 15, 2019, October 9, 2019, and January 14, 2020; accepted February 7, 2020. Date of publication February 21, 2020; date of current version July 22, 2020. This work was supported in part by the National Natural Science Foundation of China under Grant 51520105005 and Grant U1663208 and in part by the National Science and Technology Major Project of China under Grant 2017ZX05009-005 and Grant 2017ZX05049-003. *(Corresponding author: Dongxiao Zhang.)*

Yuntian Chen is with the College of Engineering, Peking University, Beijing 100871, China.

Dongxiao Zhang is with the School of Environmental Science and Engineering, Southern University of Science and Technology, Shenzhen 518055, China (e-mail: zhangdx@sustech.edu.cn).

Color versions of one or more of the figures in this article are available online at http://ieeexplore.ieee.org.

Digital Object Identifier 10.1109/TGRS.2020.2973171

In practical applications, geomechanical logs are generally predicted based on sonic logs with a certain empirical model or the first principle model to establish the geomechanical model [4], [5]. However, sonic logs are not always available, and extra costs are incurred to acquire them in addition to conventional logs. Therefore, for most wells, some conventional logs are measured and only a few wells have sonic logs (especially the shear wave velocity log), which greatly limit the accuracy of geomechanical modeling. The absence or poor quality of these log records brings great challenges for subsurface studies, which, in turn, affects numerous aspects of engineering problems, such as the design of hydraulic fracturing strategies in petroleum exploitation [3]. In shale oil and shale gas development, well completion constitutes a significant portion of the total cost, whereas approximately 30%–50% of the fracturing clusters do not contribute to production, partly due to poor completion design because of the paucity of accurate geomechanical models [6]. A common remedy is to relog the well, but this is either usually impractical or results in extremely high costs, especially when the well has been cased. Therefore, if a method for directly predicting geomechanical logs and sonic logs based on easily available conventional logs (e.g., density log and resistivity log) can be found, the cost of constructing the geomechanical model can be greatly reduced, and its accuracy can be improved. In this article, we demonstrate that an end-to-end machine learning model for directly predicting geomechanical logs based on conventional well logs can solve this problem. In this end-to-end model, neither prior information such as lithology and mineralogy nor sonic logs are required, which improves the efficiency of well log interpretation. This is an advantage over empirical models or first principle models. In addition, the physics-constrained model achieves higher accuracy by combining the physical mechanisms behind the geomechanical parameters with machine learning models.

Many researchers have attempted conventional methods to synthesize well logs, and a straightforward idea is to inspect the underlying and implicit correlations between different well logs. Certain approaches, such as cross-plot and multiple regression techniques, can be applied [7], [8]. Researchers have shown that these conventional methods are capable of predicting and synthesizing the well logs such as gamma ray (GR) [9], compensated neutron log [9], [10], density log [10], [11], and sonic logs [12]. Nevertheless, when it comes to geomechanical logs, an extremely complicated mapping exists between the nonlinearly linked input and output well logs due to the heterogeneity and complex conditions

underground [3]. Thus, conventional approaches are incapable of constructing such sophisticated relationships since they are linearly derived and naïve.

With the advent of machine learning applications in various fields of science and engineering in recent years, many researchers suggested utilizing data-driven methods, e.g., information fusion, supported vector machine (SVM), fuzzy logic models (FLMs), and artificial neural networks (ANNs), to deal with geological problems, e.g., well log estimation [13], [14], geophysical parameter estimation [15], [16], lithology characterization [1], [2], [17], [18], stratigraphic boundaries determination [19], [20], and reservoir estimation [21]. Specifically, ANN is able to discover sophisticated relationships between inputs and outputs, which is suitable for describing highly complex mappings for geomechanical log generation problems. Such merit of ANN has been acknowledged by numerous researchers, and thus, a substantial number of successful attempts have been made in the last few years. Rolon *et al.* [22] utilized the general regression neural network (GRNN) to generate synthetic well logs, and the results were compared with multiple regression. ANN and cluster analysis (CA) techniques have also been applied for well log data to estimate organic facies and burial history [23]. The genetic neural network (GNN) for wire-line log reconstruction has been presented [24], in which optimization is accomplished by a genetic algorithm instead of the traditional backpropagation (BP). Long *et al.* [25] combined a data-mining process with synthetic density log generation by ANN and demonstrated the approach with a realistic field case study. He and Misra [26] used ANNs to generate dielectric dispersion logs. Density and resistivity logs were also predicted from conventional wire-line logs by the multilayer perceptron (MLP) network [27]. However, the abovementioned neural networks may not be directly applicable to generating geomechanical logs.

The fully connected neural network (FCNN) is the most commonly used ANN, and it has been broadly applied to solving real-world engineering problems. However, the FCNN constructs a point-to-point mapping, which limits its application, especially to problems with sequence data [28]. The point-to-point mapping means that the curvilinear trend and the context information in the reservoir are neglected. However, in geological studies, the output is related to not only input at the same depth but also input that is deeper and shallower. This reflects the intuition of sequence stratigraphy. As such, the commonly used FCNN is unsuitable for the problem of log generation. A need exists for a method that can process sequence data to incorporate those geological theories into mathematical models. The recurrent neural network (RNN) is a method whose output is determined by not only the input of the current step but also the history of inputs. Thus, RNN considers the influence of the former step to the current step, and this chain-like nature of RNN constitutes its advantage in sequence data analysis over other fixed networks. RNN is the natural network architecture to use with sequence data, such as well logs.

However, the standard RNN tends to achieve poor performance when the gap between the relevant information in the previous step and the present step becomes very large [29], and long-term (spatial) dependencies exist in well logs, since the sampling intervals are relatively small and there may be a thick formation resulting from long-term deposition. Moreover, there may be a gradient vanishing problem in the standard RNN for memorizing long-term information. To solve this problem, we decide to use the long short-term memory network (LSTM), which is a particular type of RNN, which is designed to learn long-term dependencies. The LSTM has been used in the field of geoscience, such as generating nuclear magnetic resonance (NMR) distributions [30].

In [3], we demonstrated that the LSTM can learn the interaction between the upper and lower strata in the generation and autocompletion of conventional well logs and achieves superior performance over the traditional FCNN. However, generating geomechanical logs is more challenging since geomechanical logs are much more complex than traditional well logs. This problem indicates that modeling directly from the data is no longer sufficient. Therefore, we need to improve the model to better conform to physical reality. This calls for consideration of the physical mechanism behind the geomechanical logs. In this article, a two-way model is constructed, which means that the model is not a simple application of machine learning methods but rather utilizes the physical mechanism behind the engineering problem as *a priori* information. The physics-constrained neural network can directly generate geomechanical logs based on conventional well logs with higher accuracy than the traditional LSTM model. This article verifies the performance of the physics-constrained LSTM (PC-LSTM) through computational experiments based on the actual well logs from the North Dakota Williston Basin.

II. Methodology

A. Long Short-Term Memory Neural Network

An extremely complex mapping relationship exists between conventional well logs (such as GR, resistivity, and density) and geomechanical logs. To the best of the authors' knowledge, there is still no physical model that can accurately describe this mapping relationship. ANNs are capable of approximating nonlinear functional relationships between variables and can model any function up to any given precision with a sufficiently large number of basis functions [31], [32] from a mathematical perspective. This feature means that ANN possesses the potential to solve the problem of predicting geomechanical logs from conventional well logs. As discussed in Section I, RNN is more suitable for solving sequence data problems than most commonly used FCNN. At the same time, as a special RNN, LSTM is especially suitable for solving sequence data problems with long-term dependencies. Therefore, this article builds a model based on the LSTM architecture and predicts the geomechanical well logs.

The main difference between the LSTM and the standard RNN is the structure of the repeating network. The repeating network in the standard RNN is very simple, while the LSTM has four interacting layers in its repeating network, which is illustrated in Fig. 1. The top half of Fig. 1 shows the architecture of the LSTM model. The loop in the LSTM makes the model capable of remembering inputs from previous steps

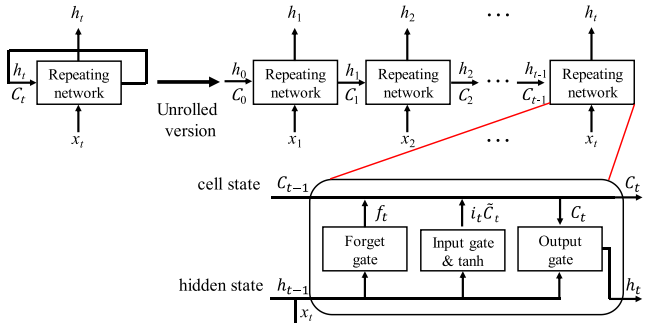

Fig. 1. Illustration of the repeating network of the LSTM.

and processing sequential data. In order to better demonstrate the architecture of LSTM, the unrolled version of this loop is also shown in Fig. 1. The bottom half shows the interacting layers in the repeating network of the LSTM.

The gates in the LSTM are used to remove or add information to the cell state, according to the hidden state of the previous step and the input of the current step. Specifically, the first gate is called forget gate, and it determines how much of the information (C_{t-1}) from the previous step should be removed (forgotten) according to (1). The input gate (2) determines what new information in the candidate ($\tilde{C}_t$) should be added in the cell state. The outputs of the following equations are numbers between zero and one, which will be multiplied with the cell state from the previous step and the candidate from the current step:

$$f_t = \sigma(W_f[h_{t-1}, x_t] + b_f) \tag{1}$$

$$i_t = \sigma(W_i[h_{t-1}, x_t] + b_i) \tag{2}$$

where h_t is the hidden state at time t; x_t is the input at time t; W and b are the weights and bias of each gate layer, respectively; the subscripts f, i, c, and o represent the forget gate layer, input gate layer, tanh layer, and output gate layer, respectively; and σ represents the activation function, which is the commonly used sigmoid function.

The third layer is a tanh layer (3), which creates a new candidate value ($\tilde{C}_t$). The output of the tanh layer provides potentially valuable information from the current steps. In (4), the old memory carried by the old cell state C_{t-1} is combined with the new candidate $\tilde{C}_t$ according to the outputs of the forget gate (1) and the input gate (2)

$$\tilde{C}_t = \tanh(W_C[h_{t-1}, x_t] + b_C) \tag{3}$$

$$C_t = f_t C_{t-1} + i_t \tilde{C}_t \tag{4}$$

where C_t is the cell state at time t, which passes through the model carrying information of previous steps, and $\tilde{C}_t$ is the candidate value that could be added to C_t.

Finally, the output of the LSTM is generated based on the updated cell state, according to the following equation in the output gate layer:

$$h_t = \sigma(W_o[h_{t-1}, x_t] + b_o) * \tanh(C_t). \tag{5}$$

By using the values of different depths in the well logs as inputs to different time steps in the LSTM, the LSTM becomes an ideal tool to generate geomechanical logs, since it is able to not only extract information from series data but also propagate information from previous time steps with long-term dependences.

B. Physics-Constrained LSTM

As discussed above, the LSTM may be an effective model since the mapping relationship between inputs and outputs is extremely complex, and geomechanical parameters are sequence data with long-term dependences. However, simply applying the LSTM model does not necessarily achieve high prediction accuracy. The existing study has proved that the domain knowledge is beneficial to break through the bottleneck of the model and further improve the prediction accuracy [33]. By combining existing background knowledge of petroleum engineering and geology, it is possible to construct an LSTM model that is more suitable for predicting geomechanical parameters. Compared with the ordinary data-driven model, the PC-LSTM model, referred to as the PC-LSTM, introduces domain knowledge as *a priori* information into the model. This kind of physics-constrained data-driven model achieves better performance since it considers the influence of the physical mechanism behind the geomechanical parameters.

Specifically, two constraints are imposed on the model, which are mechanism-mimic network architecture and formation-adjusted stratified normalization. First, by analyzing the first principle models and the empirical models for determining geomechanical parameters, it is known that the geomechanical parameters are often determined by two sonic logs that are difficult to measure [4], [5], [34]–[37]. This indicates the existence of intermediate variables in the physical models. By adding a physics-constrained layer into the LSTM network architecture, the physical mechanism behind the geomechanical parameters is introduced into the LSTM model as *a priori* information. This architecture is not similar to the conventional neural network architecture that solves such problems, and it has a stronger physical meaning. Second, the data-processing method of this model has also been improved. Simply applying the conventional normalization method often causes problems with formation misalignment and affects prediction accuracy due to the uplift and subsidence of the formation during geological evolution. By combining geological information of the stratum trend, the stratified normalization method can ensure that the target strata and the other strata of different wells remain aligned.

C. Mechanism-Mimic Network Architecture

As demonstrated by the experiments in Section III, the LSTM model is capable of generating geomechanical logs based on conventional well logs (GR, resistivity, and density). The LSTM model uses a common network architecture with two LSTM layers and two fully connected layers in front of the output layer, which is shown in Fig. 2(a). However, the direct application of the LSTM model does not necessarily achieve optimal prediction accuracy. By understanding the physical mechanisms behind the geomechanical parameters, we are able

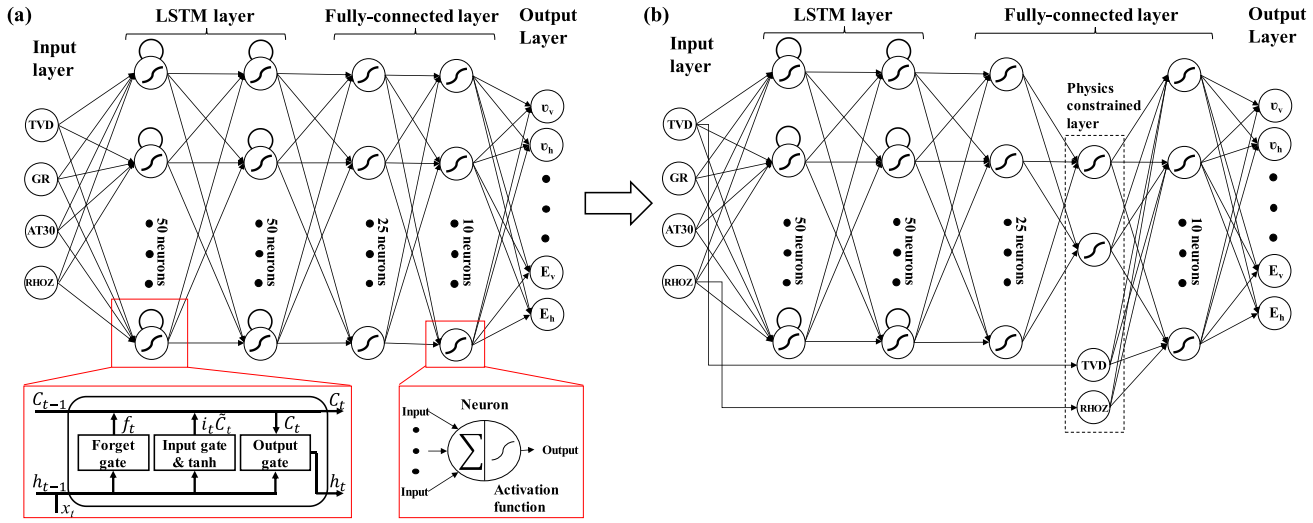

Fig. 2. LSTM architecture and the mechanism-mimic network architecture of PC-LSTM. (a) Standard LSTM architecture with two LSTM layers and two fully connected layers. (b) Mechanism-mimic network architecture of PC-LSTM. The mechanism-mimic network architecture adds a physics-constrained layer to the standard LSTM to mimic the physical mechanism of geomechanical parameters. In the mechanism-mimic network architecture, the output vector of the LSTM layer is first compressed to 2-D, and then, the tensor is combined with input variables and expanded to higher dimensions to connect the subsequent fully connected layer. The physics-constrained layer modeled after the physical mechanism enables the PC-LSTM to introduce the physical mechanism as *a priori* information by changing the network architecture.

to construct models that perform better than models that use a standard network architecture.

Concerning the mechanism-mimic network architecture, the network is adjusted according to the physical model for calculating geomechanical parameters, which is described in Appendix A. By comparing these physical models, it is found that although different geomechanical parameters are determined by different physical models, the input information of these physical models is basically derived from sonic logs (V_p and V_s), true vertical depth (TVD), and density (RHOZ). However, only the TVD and density are provided in the conventional logs, and the two sonic velocities are unknown information. Therefore, according to the physical mechanism, V_p and V_s are essentially intermediate variables of the model. Based on this assumption, a physics-constrained layer is added to the LSTM model to mimic the effects of V_p and V_s, which is shown in Fig. 2(b). In the adjusted model, the output of the LSTM layer is first passed to a fully connected layer, which is then further reduced to a 2-D vector to mimic the sonic velocities. Simultaneously, the TVD and density are directly transmitted from the input layer and combined with the 2-D vector to construct the physics-constrained layer. Finally, the physics-constrained layer is expanded to connect to the subsequent layers of the standard LSTM model.

It should be mentioned that the two neurons in the physics-constrained layer only mimic the sonic velocities but do not simulate them. In other words, adding these two neurons to the network merely constitutes a structural imitation of the physical mechanism, but these two neurons do not necessarily represent V_p and V_s. In the process of training, the two neurons are not supervised with reference to the sonic logs. Since a neural network always has a group of equivalent solutions, the two neurons in the physics-constrained layer are likely to be a set of equivalent bases (or even orthogonal bases) of V_p and V_s.

The traditional LSTM architecture is spindle-shaped, whereas the mechanism-mimic network architecture is dumbbell-shaped. The neural network generally does not perform an operation of compressing and then expanding the intermediate layer, unless for dimensionality reduction, because this will bring a loss of information. On the other hand, however, this kind of operation can also refine the information. Considering the physical mechanism behind the geomechanical parameters, this mechanism-mimic network architecture has the potential to make more accurate estimates of geomechanical parameters. Moreover, this adjustment is only for the network architecture, and the true value of V_p and V_s will not be used in the training process, which means that this adjustment does not introduce more information. This adjustment does not increase model complexity either, and the number of weights is approximately the same.

D. Formation-Adjusted Stratified Normalization

Data normalization can often improve the prediction accuracy of the model and speed-up convergence. It is important to normalize the TVD since it is not only used to track the spatial position but also helps to transfer the knowledge learned from the wells in the training data set to the wells in the test data set. The commonly used data normalization method maps the data distribution to a small interval, usually with a zero mean (by subtracting the mean in the numerator) and unit variance. However, since the well logs reflect the formation information and the formation often has a large number of undulations [Fig. 3(a)], traditional normalization methods often cause problems with formation misalignment and affect prediction accuracy [Fig. 3(b)]. Specifically, if normalization is performed for the TVD data as a whole, although the overall distribution of data is mapped into a small interval, a large deviation will exist in the distribution of the target formation (reservoir) since the target formation of different wells is always at different depths in the original TVD data.

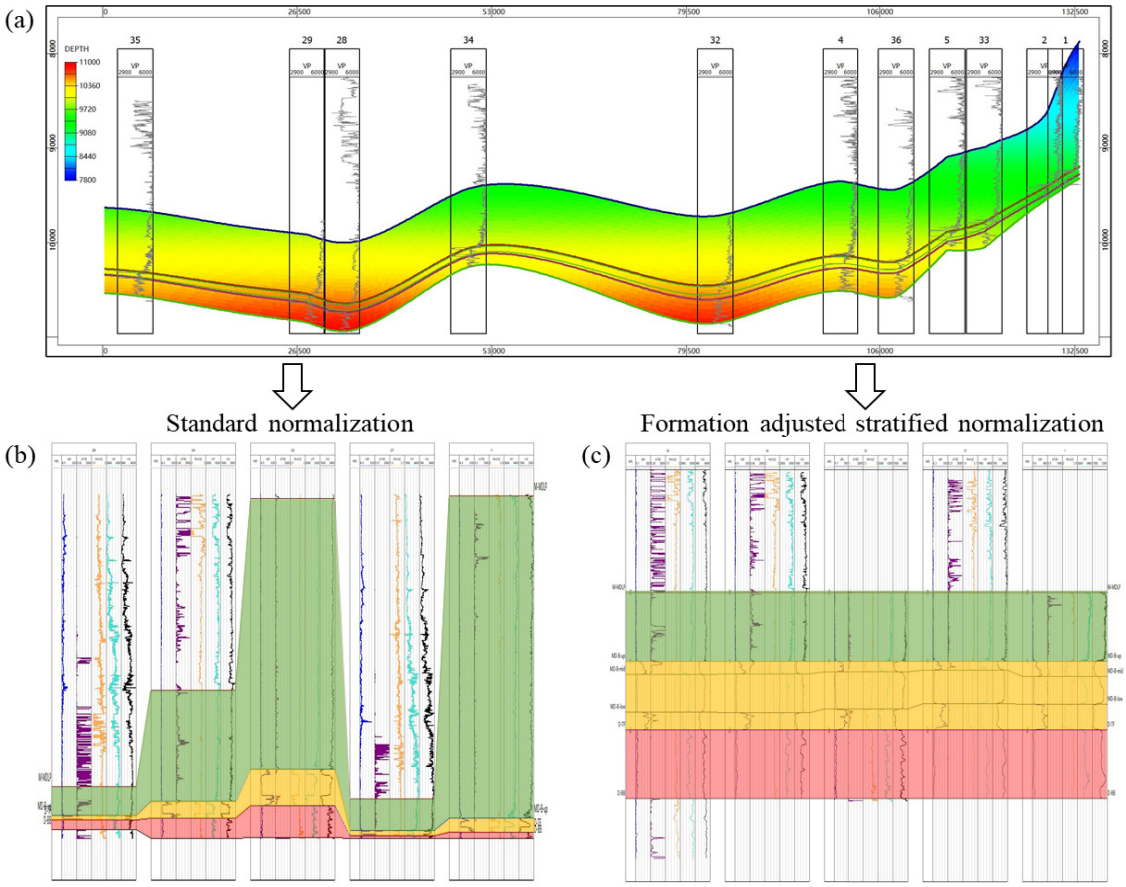

Fig. 3. Comparison of standard normalization and formation-adjusted stratified normalization. (a) Formation undulation on the West-to-East well-passing line. (b) Formation distribution after the standard normalization method. (c) Formation distribution after formation-adjusted stratified normalization.

On the other hand, if normalization is performed for the target formation, it will also result in deviations in the normalization results of other formations. Due to a large number of fluctuations in the formation, whether it is normalized for all TVD data or the target formation alone, a large deviation will exist in the normalization results.

A layered normalization method based on TVD correction is proposed to solve this dilemma. In this method, the TVD data are divided into three groups according to the target formation (i.e., Bakken formation) and its upper and lower formations (i.e., LodgePole and Three-Forks formation, respectively). The min–max normalization is applied, and the three groups of TVD data are independently mapped into different intervals, which is described in (6). In this way, it is ensured that the normalized target formations of different wells remain aligned, and the upper and lower formations are also mapped to similar intervals

$$\mathrm{TVD}_{\mathrm{norm}} = \begin{cases} \dfrac{\mathrm{TVD}-D_{\mathrm{LP,min}}}{D_{\mathrm{LP,max}}-D_{\mathrm{LP,min}}} & \text{for TVD} < D_{\mathrm{LP,\,max}} \\ \dfrac{\mathrm{TVD}-D_{\mathrm{LP,max}}}{D_{B,\mathrm{max}}-D_{\mathrm{LP,max}}}+1 & \text{for } D_{\mathrm{LP,max}} \le TVD < D_{B,\mathrm{max}} \\ \dfrac{\mathrm{TVD}-D_{B,\mathrm{max}}}{D_{\mathrm{DF,max}}-D_{B,\mathrm{max}}}+2 & \text{for TVD} > D_{B,\mathrm{max}}. \end{cases} \tag{6}$$

The effect of formation-adjusted stratified normalization is shown in Fig. 3. The LodgePole formation is represented in green, the Bakken formation is represented in yellow, and the Three-Forks formation is represented in red.

The left side is the data normalized without formation adjustment [Fig. 3(b)], and it is obvious that the formations cannot be aligned. The right side is the data stratified normalized based on TVD according to formations [Fig. 3(c)]. It is obvious that the target formation and its upper and lower formations treated by the formation-adjusted stratified normalization are more aligned among the wells on the West-to-East well-passing line than the formations treated by the standard normalization. The formation-adjusted stratified normalization constrains the data through the physical conditions of the formations, which is more in line with a physical reality. It should be mentioned that since the proposed model can process sequential data and each data point contains all the input logs at the same depth, it is not necessary to apply this adjustment to the well logs other than the TVD. It is sufficient to use the standard normalization for the other logs.

E. Physical Models for Geomechanical Log Generation

Since the geomechanical parameters are difficult to measure, the mechanical earth model (MEM) is used to generate the geomechanical fields based on sonic logs [38]. Based on the

previous research in North Dakota, an integrated workflow for calculating geomechanical parameters is developed as follows.

Assuming vertical transverse isotropy (VTI) for an anisotropic elastic medium, the M-ANNIE2 model corrected according to known core data [4], [5], is used to calculate the anisotropic elastic parameters. Based on the obtained stiffness matrix, the anisotropy Young's modulus and Poisson's ratio are calculated [34]–[36], [39]. In addition, uniaxial compressive strength (UCS) [38], [40], internal friction coefficient (μ) [36], [38], internal cohesion (C) [37], [39], [40], and tensile strength (T_0) [41], [42] are important parameters for hydraulic fracturing simulation [37]. They are estimated based on existing models according to geological information, such as the rock type and other reservoir properties. The validity of the physical model is verified by comparing the known geomechanical parameters in the database and the calculation results. In addition, the parameters obtained by the physical model are within the estimation intervals proposed by the U.S. Energy Agency through the geological survey of the area [43]. A detailed introduction of the physical models used to determine the geomechanical parameters is provided in Appendix A.

F. End-to-End Model Structure

In this article, a physics-constrained layer was added to the network architecture in order to reflect the physical mechanism behind the geomechanical parameters. This physics-constrained layer contains a 2-D vector that mimics sonic log data in geomechanical models. An end-to-end model is proposed in this article, which is capable to generate geomechanical parameters directly from conventional well logs with great accuracy.

It should be mentioned that this end-to-end model does not equal to a cascade model that simply combines a model that generates sonic logs from conventional well logs with a model that generates geomechanical parameters from sonic logs. The cascade model formed by combining the two submodels relies on sonic logs for training; however, obtaining these logs is time-consuming and expensive. In the end-to-end model, the physics-constrained layer only mimics the structure of the physical models and does not require the sonic logs for training. In addition, although the geomechanical parameters in the cascade model can be calculated from the sonic logs according to the method introduced in Appendix A, the selection of these models often depends on reservoir properties and rock types, and this information is not easily available in practice. In the end-to-end model, however, the mapping relationship between sonic logs and geomechanical parameters is completely obtained by the data-driven method and does not require geological information, such as reservoir properties and rock type. In other words, for traditional methods, different rock types require different models when calculating geomechanical logs. However, the deep learning model is more versatile, and the prior geological information such as rock types has actually been implicitly included in the geophysical logs, so there is no need to explicitly introduce such information into the model. Therefore, the end-to-end network proposed in this article can reduce the demand for input data while utilizing the physical information behind the geomechanical parameters, which is more conducive to practical applications.

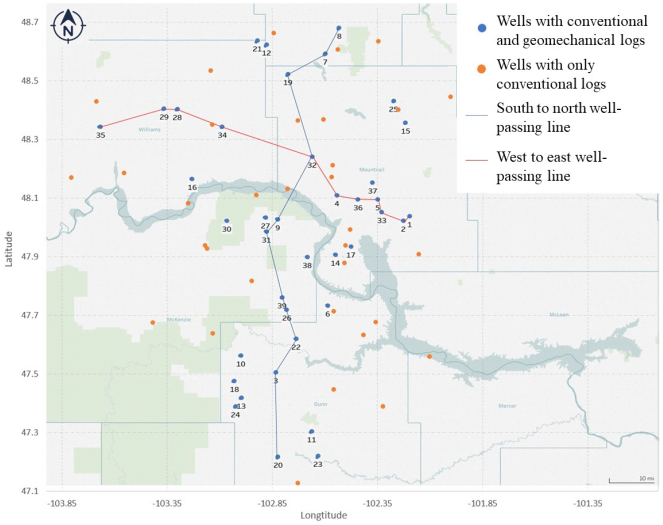

Fig. 4. Distribution of 76 wells in the North Dakota Williston Basin.

III. Experiments

A total of 76 wells from the North Dakota Williston Basin comprise the data set for this study [44]. All of the wells in the data set have conventional well logs, including GR, resistivity (AT30), and density (RHOZ), but only 39 wells contain sonic logs. This means that a full set of geomechanical logs can be constructed for these 39 wells based on the physical methods described in Appendix A. The distribution of all 76 wells is shown in Fig. 4. The blue points in Fig. 4 represent the 39 wells with both sonic logs and conventional logs. The reference geomechanical model used in subsequent experiments is obtained from these wells. The orange points are the 37 wells with only conventional logs. Due to the lack of sonic logs, conventional methods cannot use the information from these wells to build geomechanical models. The orange curve is the West-to-East well-passing line, and the blue curve is the North-to-South well-passing line. The wells on the two well-passing lines are utilized as a test data set to evaluate the model prediction accuracy in the subsequent 3-D modeling experiment.

This study evaluated the performance of the PC-LSTM model through three experiments. All of the logs are normalized in the experiments.

A. Evaluation of the Impact of Physical Constraints

In the first experiment, the effect of introducing two physical constraints is evaluated. The 39 wells with a full set of geomechanical parameters are randomly divided into a training data set (28 wells) and a test data set (11 wells). The standard LSTM model, the adjusted LSTM model with mechanism-mimic network architecture (MM-LSTM), and the PC-LSTM model with mechanism-mimic network architecture

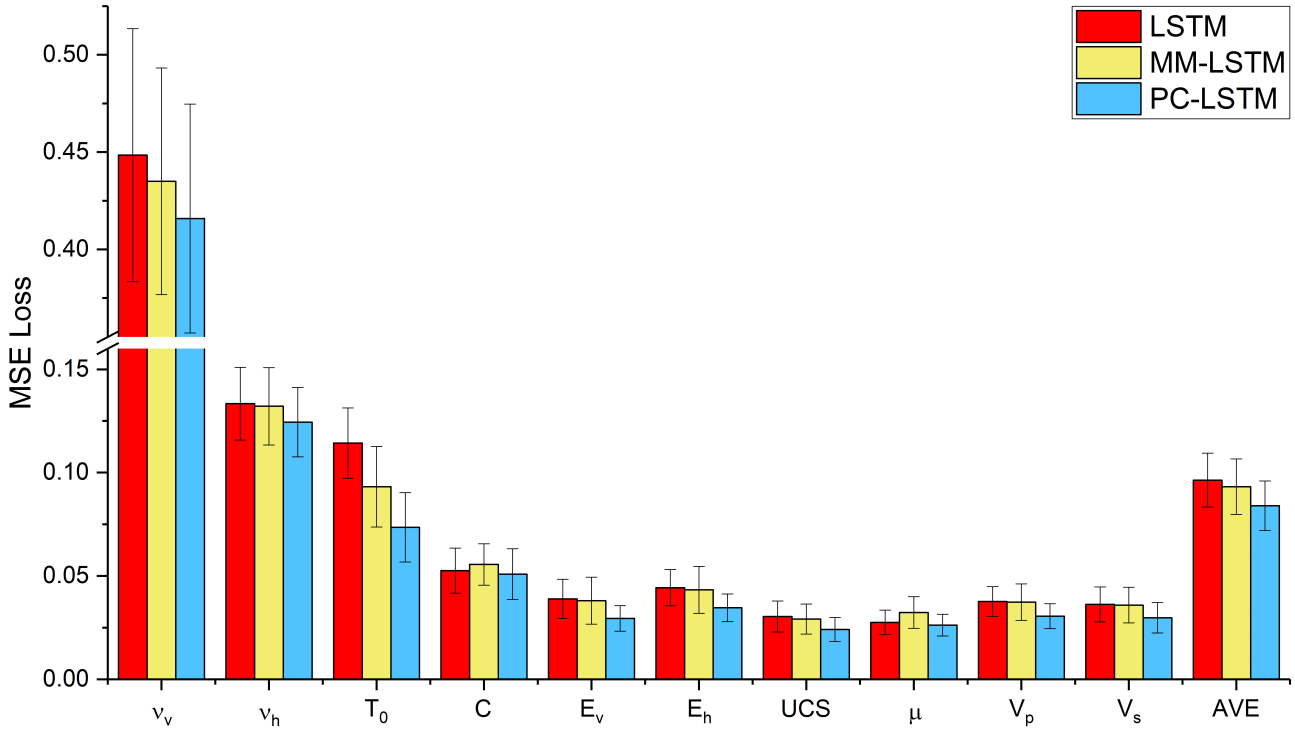

Fig. 5. Model accuracy of the standard LSTM, MM-LSTM, and PC-LSTM. The MSE losses of the ten geomechanical parameters are separately calculated, where AVE represents the average MSE loss of all geomechanical parameters. The abscissa indicates the geomechanical parameters, the ordinate is MSE, and the error bar indicates the MSE standard deviation of 20 independent experiments.

and formation-adjusted normalization (PC-LSTM) are separately trained with the training data set and compared with the test data set. The experiment is repeated 20 times to avoid randomness affecting the statistical results, and the training data set and the test data set are reallocated each time. The prediction results of different models are evaluated based on the mean-square-error (MSE) function.

The results of 20 independent experiments of the three models are shown in Fig. 5. Fig. 5 shows the prediction MSE loss of different geomechanical parameters for the standard LSTM (red), MM-LSTM (yellow), and PC-LSTM (blue) models. The error bars represent the standard deviation of the MSE loss obtained from 20 random experiments. The specific values in the histogram are shown in Table I, which are the MSE loss plus or minus standard deviation of the prediction results of the three models for each geomechanical parameter. AVE represents the average MSE loss of all predictors. The lower the values, the more accurate and stable is the model. The minimum value of each group is shown in bold. The network architecture of MM-LSTM is improved according to the physical mechanism, and PC-LSTM is a model that considers both physical constraints of network architecture and formation-adjusted stratified normalization. The three models in Fig. 5 have a similar model complexity and the same input information, and thus, the difference in model accuracy depends on whether the physical mechanism is considered. As shown in Table I and Fig. 5, the average MSE loss of the PC-LSTM is reduced by 12.5% compared to the standard LSTM with a smaller error standard deviation, thus indicating that the PC-LSTM proposed in this article can not only improve the accuracy of the model but also reduce the uncertainty of the prediction results. In addition, an interesting phenomenon was discovered through experiments. If only one physics-constraint is added to the model, the average MSE is only reduced by 3.3% for the mechanism-mimic network architecture and 3.2% for the formation-adjusted stratified normalization. But when both physics constraints are introduced at the same time, the average MSE is reduced by 12.5%. This indicates that the effects of physics-constraints are not linearly additive but have a mutually reinforcing effect. The comparison results in Fig. 5 show that the PC-LSTM based on the physical mechanism achieves superior performance.

TABLE I
MSE LOSS OF LSTM, MM-LSTM, AND PC-LSTM

	LSTM	MM-LSTM	PC-LSTM
ν_v	0.448±0.065	0.435±0.058	**0.416±0.059**
ν_h	0.133±0.018	0.132±0.019	**0.124±0.017**
T_0	0.114±0.017	0.093±0.019	**0.074±0.017**
C	0.053±0.011	0.056±0.010	**0.051±0.012**
E_v	0.039±0.009	0.038±0.011	**0.029±0.006**
E_h	0.044±0.009	0.043±0.011	**0.035±0.007**
UCS	0.030±0.007	0.029±0.007	**0.024±0.006**
μ	0.028±0.006	0.032±0.008	**0.026±0.005**
ν_p	0.038±0.007	0.037±0.009	**0.031±0.006**
ν_s	0.036±0.008	0.036±0.009	**0.030±0.007**
AVE	0.096±0.013	0.093±0.013	**0.084±0.012**

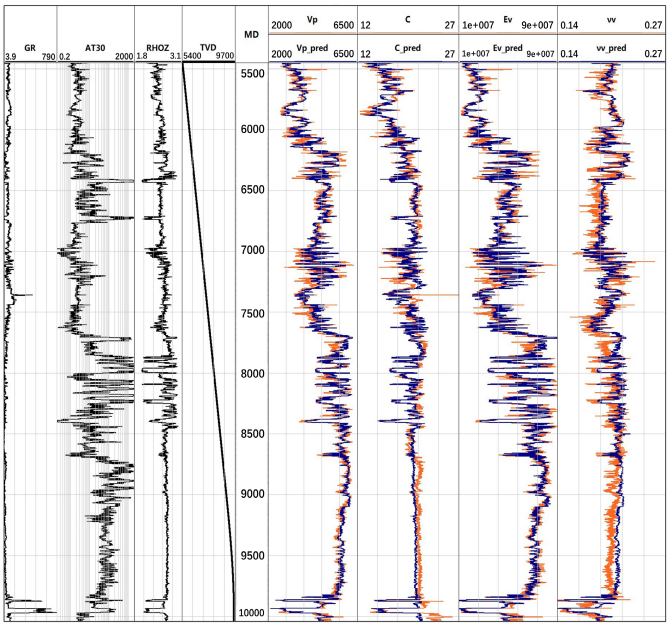

Fig. 6. Prediction results of the No. 5 well, including compressional velocity V_p, cohesion C, vertical Young's modulus E_{v}, and vertical Poisson's ratio ν_{v}.

The MSE is a commonly used indicator in machine learning to measure the model performance, but it is relatively abstract from the engineering perspective. In order to reflect the model performance more directly, the absolute error is calculated. In the proposed model, a total of ten different logs are generated, including V_p, V_s, T_0, C, UCS, μ, E_{v}, E_{h}, ν_{v}, and ν_{h}, and their corresponding absolute errors are 2.9%, 3.3%, 6.9%, 2.4%, 3.2%, 2.3%, 5.7%, 4.8%, 2.9%, and 2.6%, respectively. The overall average absolute error of all the ten well logs is 3.7%.

The specific prediction results are shown in Fig. 6. Considering space limitations, only one well prediction result from one experiment is randomly selected here, and its prediction results are displayed. Fig. 6 shows the prediction results of the geomechanical parameters compressional velocity V_p, cohesion C, vertical Young's modulus E_{v}, and vertical Poisson's ratio ν_{v}, in order. The input variables are the GR, resistivity AT30, density RHOZ, and TVD. The MD represents the measured depth. The left side of the MD shows the input variables, and the right side shows the output variables. The yellow curves represent the true values, and the blue curves represent the predicted values. For well logs, valuable information is stored in the trend information of the data, and absolute values are not important. By comparing the actual geomechanical parameters and predicted values, PC-LSTM is capable of predicting the trend of geomechanical parameters more accurately, which is critical for practical applications. These predictions are useful for establishing a more accurate geomechanical model, improving reservoir evaluation accuracy, and optimizing well drilling and completion strategies.

B. 3-D Geomechanical Field Generation Experiment

The second experiment demonstrates the effect of the PC-LSTM on improving the accuracy of geomechanical modeling in practical applications. Full-field 3-D models on geomechanical parameters are built based on model predictions in this experiment. The modeling method based on geomechanical parameters is provided in Appendix B. In order to make the experiment more in line with the actual situation and more challenging, the test wells were not randomly selected, but the 21 wells were selected as test data from the widest part of the West-to-East direction and the South-to-North direction of the distribution of 39 wells. The distribution of test wells is shown in Fig. 4. In this way, the test data account for more than half of all available data, and the whole field is divided into four parts, which not only increases the difficulty of the problem but also simulates the uneven distribution of wells with complete logging information in the real-world development. The full-field 3-D models generated in this experiment are shown in Fig. 7. Fig. 7(a) presents the model generated based on the 18 available wells (training data set); Fig. 7(b) shows the model constructed based on the predictions of the geomechanical parameters of the unknown wells (test data set) through the PC-LSTM; and Fig. 7(c) presents the reference model, which is generated based on a total of 39 wells with a full set of geomechanical log data. Since Fig. 7(c) is the reference model, the closer the results of Fig. 7(b) and (c) are to Fig. 7(a), the more effective is the corresponding method.

By comparing the geomechanical modeling results, it is shown that great similarity exists between the full-field 3-D model constructed based on the PC-LSTM predictions [Fig. 7(b)] and the reference model based on the geomechanical parameters of all 39 wells [Fig. 7(c)]. This indicates that PC-LSTM can effectively extract the mapping relationship between geomechanical parameters and conventional well logs and generate physical fields similar to reference fields. The application of the PC-LSTM is capable of improving the accuracy of geomechanical modeling. In addition, the attribute distribution on the surface of each formation shows that conventional models, such as kriging, have difficulty in predicting data spatially far from known data. However, data could be accurately predicted by the PC-LSTM, as long as they are located in similar geological settings with known data. In fact, spatial distance does not determine the accuracy of the PC-LSTM, which constitutes an advantage of the PC-LSTM over other conventional methods.

C. Building-Extended Geomechanical Fields Based on PC-LSTM

As the first two experiments validate the effectiveness of the PC-LSTM, an advanced workflow could be introduced at this point. Specifically, if a conventional well log is available, sonic logs and geomechanical parameters could be obtained based on the PC-LSTM. In addition, a more accurate geomechanical field could be constructed based on the estimations, which is helpful for geological analysis and reservoir simulation.

The third experiment is a demonstration of the usefulness of this workflow, in which the PC-LSTM is utilized to predict the geomechanical parameters of the unmeasured wells in the North Dakota Williston Basin region. Specifically,

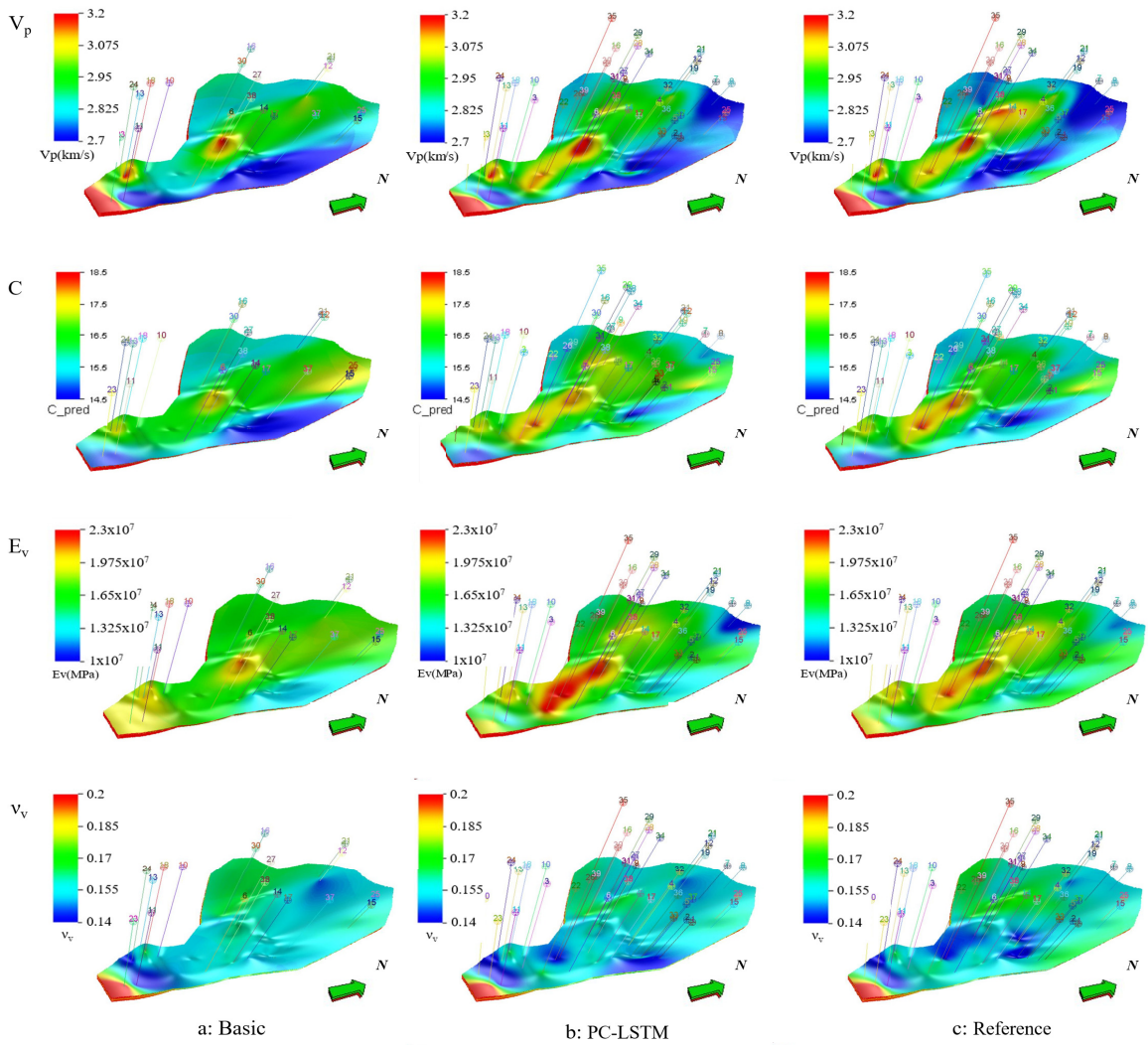

Fig. 7. Full-field 3-D models on geomechanical parameters. The compressional velocity field (V_p), cohesion (C), vertical Young's modulus field (E_v), and vertical Poisson's ratio field (ν_v) generated based on different models. (a) Basic fields generated based on available training wells through traditional geomechanical modeling methods. (b) Geomechanical fields generated based on the training wells and the prediction of test wells via PC-LSTM. (c) Reference fields generated based on all 39 wells.

as mentioned above, there are 37 wells that only contain conventional well logs (GR, AT30, and RHOZ) but no sonic logs or geomechanical logs. With these data, the PC-LSTM can be utilized to generate geomechanical logs. The PC-LSTM is first trained based on the 39 wells with geomechanical logs. Then, the geomechanical parameters of the 37 wells with only conventional well logs are predicted. Finally, a more detailed geomechanical model of the Williston Basin area of North Dakota is built based on geomechanical logs from all 76 wells. It should be mentioned that although these 37 wells are geographically located outside of the area covered by the training data set, they are in the same basin covered by the training data set from a geological perspective. Therefore, the 37 wells may be predicted by the model trained by 39 wells.

By applying the PC-LSTM, more detailed geomechanical information could be obtained with high accuracy. Since the 76 wells cover a larger area than the 39 wells, modeling the 76 wells using the PC-LSTM can not only improve the geomechanical modeling accuracy but also extend the coverage of geomechanical models. It is shown in Fig. 8(b) that the geomechanical model generated from the 76 wells is more elaborate and larger than the reference model constructed based on the 39 wells [Fig. 8(a)]. For example, the low-velocity zone in the V_p field located in the Southwest of the research area is not shown in the reference model since it is out of range, but it is detected in the extended model based on the PC-LSTM. The application of the PC-LSTM makes it possible to extract information from samples lacking sonic logs, expand the geomechanical parameter data set, and construct geomechanical parameter fields with wider coverage and more detailed description. With the PC-LSTM, more well logs could be used for geomechanical analysis. The PC-LSTM provides an efficient way to make full use of economically available conventional well logs to generate more accurate geomechanical models. With more data being

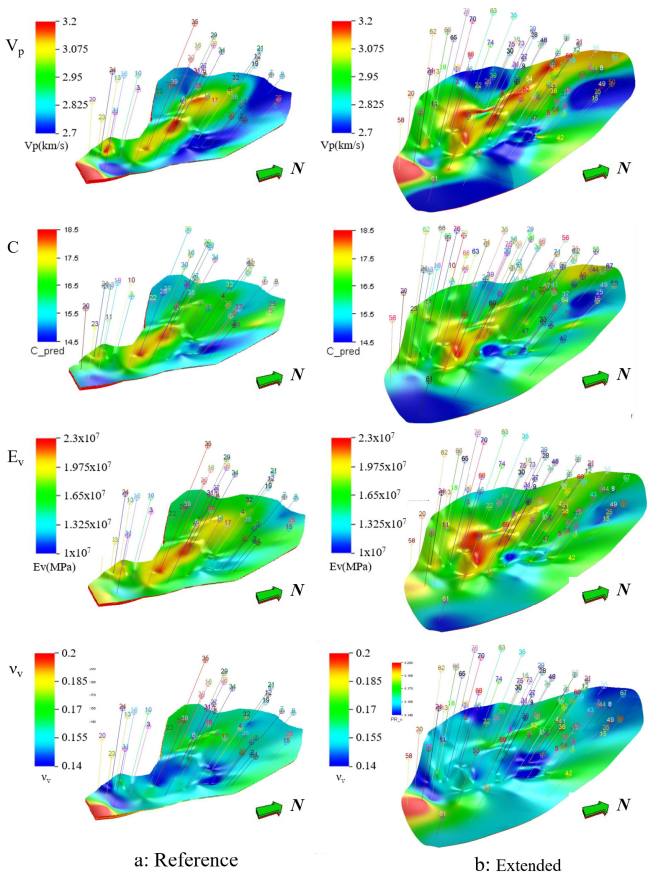

Fig. 8. Reference and extended full-field 3-D models on geomechanical parameters. The compressional velocity field (V_p), cohesion (C), vertical Young's modulus field (E_v), and vertical Poisson's ratio field (ν_v) generated based on different models. (a) Reference fields generated based on all 39 wells. (b) Extended fields generated based on 76 wells via PC-LSTM.

taken into account, risks involved in decision-making for oil field development could be substantially reduced.

IV. Conclusion

The physics-constrained neural network proposed in this article can accurately generate geomechanical logs at a low cost based on readily available conventional logs, which brings a significant value to the subsurface. These geomechanical logs greatly benefit subsurface description, reservoir evaluation, and exploration of underground resources, such as oil and gas, groundwater, minerals, and geothermal energy.

Through this study, we showed that the process of applying machine learning methods to engineering practice is not one way but rather should be two ways. In fact, the physical mechanism behind the engineering problem is very important to improve the performance of the machine learning model. By analyzing the physical mechanism behind the problem and introducing it as *a priori* information, a machine learning model that is more suitable for the problem can be constructed. Through this two-way mechanism, the characteristics of the problem itself can be used to feed back the model and improve its performance. Specifically, two constraints are imposed on the model, which are mechanism-mimic network architecture and formation-adjusted stratified normalization.

It should be mentioned that the PC-LSTM model in this study is not a surrogate model for the first principle models and empirical models that determine the geomechanical parameters. Usage of these first principle models and empirical models depends on geological information, such as rock type and reservoir properties, which is not contained in the input variables in this study. Thus, with such information, it would be difficult to directly calculate the geomechanical parameters based on first principle models and empirical models. The physics-constrained data-driven model proposed in this study is an end-to-end model, which means that the feature engineering is not required. This model is capable of describing the direct mapping relationship between conventional well logs and geomechanical parameters; thus, it can be used to generate geomechanical logs based on conventional well logs. This physics-constrained model helps to reduce the logging cost and increase the accuracy of geomechanical modeling and brings value to the subsurface.

Appendix A

A. Physical Models for Geomechanical Well Log Generation

In order to calculate the geomechanical parameters, the stiffness tensor needs to be calculated first. Assuming VTI for an anisotropic elastic medium, the tensor could be represented as follows:

$$\{C_{ij}\} = \begin{bmatrix} C_{11} & C_{12} & C_{13} & 0 & 0 & 0 \\ C_{12} & C_{11} & C_{13} & 0 & 0 & 0 \\ C_{13} & C_{13} & C_{33} & 0 & 0 & 0 \\ 0 & 0 & 0 & C_{44} & 0 & 0 \\ 0 & 0 & 0 & 0 & C_{44} & 0 \\ 0 & 0 & 0 & 0 & 0 & C_{66} \end{bmatrix}. \quad \text{(A.1)}$$

Using compressional velocity (V_p), shear velocity (V_s), and density, C_{33} and C_{44} can be determined by (A.2) and (A.3), respectively. The M-ANNIE2 model [5] is applied for calculating C_{66}, C_{11}, C_{12}, and C_{13}

$$C_{33} = \rho V_p^2 \quad \text{(A.2)}$$

$$C_{44} = \rho V_s^2 \quad \text{(A.3)}$$

$$C_{66} = \frac{2k_1 \frac{C_{44}}{C_{33}} + 1 - k_1 - k_3}{2k_1 \frac{1}{C_{33}} - k_3 \frac{1}{C_{44}}} \quad \text{(A.4)}$$

$$C_{11} = k_1(2C_{66} - 2C_{44} + C_{33}) \quad \text{(A.5)}$$

$$C_{12} = C_{11} - 2C_{66} \quad \text{(A.6)}$$

$$C_{13} = k_2 C_{12} \quad \text{(A.7)}$$

where k_1, k_2, and k_3 are empirical properties derived from core data, which matches with most databases.

Young's modulus (E) is the ratio of longitudinal stress to longitudinal strain. Poisson's ratio (υ) is the ratio of latitudinal to longitudinal strain. The anisotropic Young's modulus and Poisson's ration are calculated based on the elements of the stiffness tensor [34]–[36], [39]

$$E_h = \frac{(C_{11} - C_{12})\left[C_{33}(C_{11} + C_{12}) - 2C_{13}^2\right]}{C_{11}C_{33} - C_{13}^2} \quad \text{(A.8)}$$

$$E_v = C_{33} - \frac{2C_{13}^2}{C_{11} + C_{12}} \quad \text{(A.9)}$$

$$v_h = \frac{C_{33}C_{12} - C_{13}^2}{C_{33}C_{11} - C_{13}^2} \tag{A.10}$$

$$v_v = \frac{C_{13}}{C_{11} + C_{12}}. \tag{A.11}$$

UCS describes the maximum axial compressive stress that a right-cylindrical sample of material can withstand before failing. There are three layers in the target formation Bakken: upper, middle, and lower. For each specific layer, we applied different empirical equations for calculating UCS [35]. For the upper and lower layers, which are organic-rich shales, (A.12) is applied. (A.13) is used for the middle layer, which is mainly limestone

$$\text{UCS} = 7.22E_{\text{stat}}^{0.712} \tag{A.12}$$

$$\text{UCS} = 13.8E_{\text{stat}}^{0.51}. \tag{A.13}$$

For the other formation, empirical equations developed by Bradford *et al.* [40] are applied for calculating UCS, which is used worldwide for UCS $>$ 700 psi

$$\text{UCS} = 2.28 + 4.1089E_{\text{stat}}. \tag{A.14}$$

Internal friction factor (μ), also called the internal friction angle, is a measure of the ability of a unit of rock to withstand a shear stress. It is the angle (μ) measured between the normal force and resultant force, which is attained when failure just occurs in response to a shearing stress. The internal friction factor is an important parameter for hydraulic fracturing simulation [37], and it is calculated as follows [41]:

$$\mu = 26.5 - 37.4(1 - \varphi - V_{\text{shale}}) + 62.1(1 - \varphi - V_{\text{shale}}^2). \tag{A.15}$$

For the Bakken formation, the shale rock from upper and lower layers exhibits different characteristics. The empirical equation for the upper and lower layers is calculated as follows [38]:

$$\mu = 18.352V_p^{0.5148}. \tag{A.16}$$

Cohesion (C) is the resistance force per unit area if a shear force is applied to a cube of rock at zero normal pressure. It is mainly controlled by the lithology and mineralogy, and the following equations determine cohesion for limestone, shale, and sandstone [45]–[47]:

$$C = \begin{cases} \dfrac{\text{UCS}}{2}\dfrac{(1-\sin\mu)}{\cos\mu} & \text{limestone} \\ 10\tan\mu & \text{shale} \\ \dfrac{\text{UCS}}{2\tan\left(\frac{\pi}{4} + \frac{\mu}{4}\right)} & \text{sandstone.} \end{cases} \tag{A.17}$$

Tensile strength (T_0) refers to the force per unit cross-sectional area required to pull a substance apart. It is also an important parameter describing rock strength [37]. For different lithologies, different empirical equations are applied as follows [41], [42]:

$$T_0 = \begin{cases} 0.1\text{UCS} & \text{shale} \\ \left(\dfrac{\text{UCS}}{9.25}\right)^{\frac{1}{0.947}} & \text{limestone.} \end{cases} \tag{A.18}$$

APPENDIX B

B. Geomechanical Modeling Based on Geomechanical Parameters

Regarding the geomechanical model generation process, modeling based on the interpolation of well logs and formation tops is conducted. Well location is set using the longitude and latitude provided by the database. Since the Williston Basin is a large intracratonic sedimentary basin with no giant fault zones existing in the research area, fault modeling is not required [38]. Different interpolation methods are used according to different purposes. The thin-plate spline interpolation algorithm is applied for horizon modeling to generate a relatively smooth formation surface. Under the XY gridding model, constrained by the Mississippian-LodgePole formation top and Devonian-Birdbear formation top, the zone models of LodgePole, Bakken, and Three-Forks formations are set up. Upscaled well logs and geomechanical logs of each formation are calculated by square root average and are extracted to the grid. A physical property modeling process was implemented to compute geomechanical maps. The ordinary kriging algorithm is selected in order to generate attribute models constrained by formations. Each modeling process used the same set of hyperparameters for interpolation. As a result, 3-D geomechanical models are built and could be viewed from the surface slice to observe the distributions of geomechanical properties.

ACKNOWLEDGMENT

The authors are grateful to Mr. Jiawei Yan for his assistance with data preparation, figure generation, and constructive discussions during the course of this article.

REFERENCES

[1] R. Feng, S. M. Luthi, D. Gisolf, and E. Angerer, "Reservoir lithology determination by hidden Markov random fields based on a Gaussian mixture model," *IEEE Trans. Geosci. Remote Sens.*, vol. 56, no. 11, pp. 6663–6673, Nov. 2018.

[2] H.-C. Chang, H.-C. Chen, and J.-H. Fang, "Lithology determination from well logs with fuzzy associative memory neural network," *IEEE Trans. Geosci. Remote Sens.*, vol. 35, no. 3, pp. 773–780, May 1997.

[3] D. Zhang, Y. Chen, and J. Meng, "Synthetic well logs generation via recurrent neural networks," *Petroleum Explor. Develop.*, vol. 45, no. 4, pp. 629–639, Aug. 2018.

[4] J. F. Nye, *Physical Properties of Crystals: Their Representation by Tensors and Matrices*. London, U.K.: Oxford Univ. Press, 1985.

[5] E. Murphy, S. R. Barraza, M. Gu, D. Gokaraju, M. E. Far, and J. Quirein, "New models for acoustic anisotropic interpretation in shale," in *Proc. SPWLA 56th Annu. Logging Symp.*, 2015, pp. 1–15.

[6] J. Parshall, "Drilling data provide solution to horizontal well log costs," *J. Petroleum Technol.*, vol. 67, no. 8, pp. 35–38, Aug. 2015.

[7] H. Eskandari, M. Rezaee, and M. Mohammadnia, "Application of multiple regression and artificial neural network techniques to predict shear wave velocity from wireline log data for a carbonate reservoir South-West Iran," *CSEG Recorder*, vol. 42, p. 48, Sep. 2004.

[8] W. Wendt, S. T. Sakurai, and P. Nelson, *Permeability Prediction From Well Logs Using Multiple Regression*. Amsterdam, The Netherlands: Elsevier, 1986.

[9] C. Cheng and T. Liang, "Digital processing methods based on the old logging series," *Natural Gas Ind.*, vol. 28, no. 1, pp. 67–69, 2008.

[10] J. Wang, L. Liang, Q. Deng, P. Tian, and W. Tan, "Research and application of log reconstruction based on multiple regression model," *Lithologic Reservoirs*, vol. 28, no. 3, pp. 113–120, 2016.

[11] M. Liao, "The application of multiple regression method to the calibration of the influence of hole enlargement on density and acoustic logs," *Geophys. Geochem. Explor.*, vol. 38, no. 1, pp. 174–179, 2014.

[12] F. D. O. A. Augusto and J. L. Martins, "A well-log regression analysis for P-wave velocity prediction in the namorado oil field, Campos basin," *Revista Brasileira de Geofisica*, vol. 27, no. 4, pp. 595–608, May 2010.

[13] S. Soltani, M. Kordestani, P. K. Aghaee, and M. Saif, "Improved estimation for well-logging problems based on fusion of four types of Kalman filters," *IEEE Trans. Geosci. Remote Sens.*, vol. 56, no. 2, pp. 647–654, Feb. 2018.

[14] B. Zhou, S. Fraser, M. Borsaru, T. Aizawa, R. Sliwa, and T. Hashimoto, "New approaches for rock strength estimation from geophysical logs," in *Proc. Bowen Basin Symp.*, 2005, pp. 151–164.

[15] A. A. Zerrouki, T. Aïfa, and K. Baddari, "Prediction of natural fracture porosity from well log data by means of fuzzy ranking and an artificial neural network in Hassi Messaoud oil field, Algeria," *J. Petroleum Sci. Eng.*, vol. 115, pp. 78–89, Mar. 2014.

[16] U. Iturrarán-Viveros and J. O. Parra, "Artificial neural networks applied to estimate permeability, porosity and intrinsic attenuation using seismic attributes and well-log data," *J. Appl. Geophys.*, vol. 107, pp. 45–54, Aug. 2014.

[17] G. Wang, T. R. Carr, Y. Ju, and C. Li, "Identifying organic-rich Marcellus Shale lithofacies by support vector machine classifier in the Appalachian basin," *Comput. Geosci.*, vol. 64, pp. 52–60, Mar. 2014.

[18] A. A. Silva, I. A. L. Neto, R. M. Misságia, M. A. Ceia, A. G. Carrasquilla, and N. L. Archilha, "Artificial neural networks to support petrographic classification of carbonate-siliciclastic rocks using well logs and textural information," *J. Appl. Geophys.*, vol. 117, pp. 118–125, Jun. 2015.

[19] U. K. Singh, "Fuzzy inference system for identification of geological stratigraphy off Prydz Bay, East Antarctica," *J. Appl. Geophys.*, vol. 75, no. 4, pp. 687–698, Dec. 2011.

[20] K. Silversides, A. Melkumyan, D. Wyman, and P. Hatherly, "Automated recognition of stratigraphic marker shales from geophysical logs in iron ore deposits," *Comput. Geosci.*, vol. 77, pp. 118–125, Apr. 2015.

[21] Y. Chen, S. Jiang, D. Zhang, and C. Liu, "An adsorbed gas estimation model for shale gas reservoirs via statistical learning," *Appl. Energy*, vol. 197, pp. 327–341, Jul. 2017.

[22] L. Rolon, S. D. Mohaghegh, S. Ameri, R. Gaskari, and B. Mcdaniel, "Using artificial neural networks to generate synthetic well logs," *J. Natural Gas Sci. Eng.*, vol. 1, nos. 4–5, pp. 118–133, Nov. 2009.

[23] B. Alizadeh, S. Najjari, and A. Kadkhodaie-Ilkhchi, "Artificial neural network modeling and cluster analysis for organic facies and burial history estimation using well log data: A case study of the South Pars gas field, Persian Gulf, Iran," *Comput. Geosci.*, vol. 45, pp. 261–269, Aug. 2012.

[24] X. Mo, Q. Zhang, and X. Li, "Well logging curve reconstruction based on genetic neural networks," in *Proc. 12th Int. Conf. Fuzzy Systems Knowl. Discovery (FSKD)*, Aug. 2015, pp. 1015–1021.

[25] W. Long, D. Chai, and F. Aminzadeh, "Pseudo density log generation using artificial neural network," in *Proc. SPE Western Regional Meeting*, 2016, pp. 1–21.

[26] J. He and S. Misra, "Generation of synthetic dielectric dispersion logs in organic-rich shale formations using neural-network models," *Geophysics*, vol. 84, no. 3, pp. D117–D129, May 2019.

[27] M. M. Salehi, M. Rahmati, M. Karimnezhad, and P. Omidvar, "Estimation of the non records logs from existing logs using artificial neural networks," *Egyptian J. Petroleum*, vol. 26, no. 4, pp. 957–968, Dec. 2017.

[28] A. Karpathy. *The Unreasonable Effectiveness of Recurrent Neural Networks*. Accessed: Feb. 1, 2020. [Online]. Available: http://karpathy.github.io/2015/05/21/rnn-effectiveness/

[29] Y. Bengio, P. Simard, and P. Frasconi, "Learning long-term dependencies with gradient descent is difficult," *IEEE Trans. Neural Netw.*, vol. 5, no. 2, pp. 157–166, Mar. 1994.

[30] H. Li and S. Misra, "Long short-term memory and variational autoencoder with convolutional neural networks for generating NMR T2 distributions," *IEEE Geosci. Remote Sens. Lett.*, vol. 16, no. 2, pp. 192–195, Feb. 2019.

[31] G. Cybenko, "Approximation by superpositions of a sigmoidal function," *Math. Control Signal Syst.*, vol. 2, no. 4, pp. 303–314, 1989.

[32] K. Hornik, "Approximation capabilities of multilayer feedforward networks," *Neural Netw.*, vol. 4, no. 2, pp. 251–257, 1991.

[33] Y. Chen, H. Chang, J. Meng, and D. Zhang, "Ensemble Neural Networks (ENN): A gradient-free stochastic method," *Neural Netw.*, vol. 110, pp. 170–185, Feb. 2019.

[34] S. M. Higgins, S. A. Goodwin, A. Donald, T. R. Bratton, and G. W. Tracy, "Anisotropic stress models improve completion design in the Baxter Shale," in *Proc. SPE Annu. Tech. Conf. Exhib.*, 2008, pp. 1–10.

[35] T. Lo, K. B. Coyner, and M. N. Toksöz, "Experimental determination of elastic anisotropy of Berea sandstone, Chicopee shale, and Chelmsford granite," *Geophysics*, vol. 51, no. 1, pp. 164–171, Jan. 1986.

[36] A. S. Wendt *et al.*, "Advanced mechanical earth modelling and wellbore-stability calculation using advanced sonic measurements: A case study on an HP/HT field in the Norwegian North Sea," in *Proc. SPE Annu. Tech. Conf. Exhib.*, 2007, pp. 1–16.

[37] H. Tang, S. Li, and D. Zhang, "The effect of heterogeneity on hydraulic fracturing in shale," *J. Petroleum Sci. Eng.*, vol. 162, pp. 292–308, Mar. 2018.

[38] M. Ostadhassan, Z. Zeng, and S. Zamiran, "Geomechanical modeling of an anisotropic formation-Bakken case study," in *Proc. 46th US Rock Mech./Geomech. Symp.*, 2012, pp. 1–15.

[39] M. King, "Static and dynamic elastic moduli of rocks under pressure," in *Proc. 11th US Symp. Rock Mech. (USRMS)*, 1969, pp. 1–24.

[40] I. D. R. Bradford, J. Fuller, P. J. Thompson, and T. R. Walsgrove, "Benefits of assessing the solids production risk in a North Sea reservoir using elastoplastic modelling," in *Proc. SPE/ISRM Rock Mech. Petroleum Eng.*, 1998, pp. 261–269.

[41] A. Alexeyev *et al.*, "Well log based geomechanical and petrophysical analysis of the Bakken formation," in *Proc. 51st US Rock Mech./Geomech. Symp.*, 2017, pp. 1–9.

[42] A. Asadi, "Application of artificial neural networks in estimation of uniaxial compressive strength using indirect tensile strength data of limestone rocks," in *Proc. ISRM Regional Symp.-EUROCK*, 2015, pp. 1–6.

[43] C. Wang and Z. Zeng, "Overview of geomechanical properties of Bakken formation in Williston Basin, North Dakota," in *Proc. 45th US Rock Mech./Geomech. Symp.*, 2011, pp. 1–11.

[44] *Well File Database*, NDIC, Bismarck, ND, USA, 2018.

[45] N. Tokashiki and O. Aydan, "Estimation of rockmass properties of Ryukyu limestone," in *Proc. ISRM Regional Symp.-7th Asian Rock Mech. Symp.*, 2012, pp. 1–10.

[46] M. A. Bagheri and A. Settari, "Modeling of geomechanics in naturally fractured reservoirs," *SPE Reservoir Eval. Eng.*, vol. 11, no. 1, pp. 108–118, Feb. 2008.

[47] L. Sousa, Jr., E. Santos, and F. Ferreira, "Geomechanical data acquisition and modeling applied to an offshore sandstone petroleum reservoir," in *Proc. 44th US Rock Mech. Symp. 5th US-Canada Rock Mech. Symp.*, 2010, pp. 1–12.

Yuntian Chen received the B.S. degree from the Department of Energy and Power Engineering, Tsinghua University, Beijing, China, in 2015. He is currently pursuing the Ph.D. degree in energy and resource engineering with Peking University, Beijing.

He was a Research Intern with the School of Engineering and Applied Sciences, Harvard University, Cambridge, MA, USA, and also with the Development Research Center of the State Council, Beijing, in 2014 and 2015, respectively. His research interests include statistical modeling, inverse modeling, and machine learning in petroleum engineering.

Dongxiao Zhang received the M.S. and Ph.D. degrees in hydrology from the University of Arizona, Tucson, AZ, USA, in 1992 and 1993, respectively.

From 1996 to 2003, he was a Technical Staff Member and the Team Leader with the Los Alamos National Laboratory, Los Alamos, NM, USA. From 2004 to 2007, he was the Miller Chair Professor of petroleum and geological engineering with the University of Oklahoma, Norman, OK, USA. From 2007 to 2010, he was the Marshall Professor of the Petroleum Engineering Program with the University of Southern California, Los Angeles, CA, USA. From 2010 to 2019, he was the Chair Professor and the Dean of the College of Engineering, Peking University, Beijing, China. He is currently the Provost and the Chair Professor with the Southern University of Science and Technology, Shenzhen, China. He has authored *Stochastic Methods for Flow in Porous Media* and more than 180 articles. His research interests include stochastic uncertainty quantification and inverse modeling, mechanisms for shale–gas and coalbed–methane production, and geological carbon sequestration.

Dr. Zhang is a member of the U.S. National Academy of Engineering, a fellow of the Geological Society of America, and an Honorary Member of the Society of Petroleum Engineers.